Transition Metal Modified TiO_2-Loaded MCM-41 Catalysts for Visible- and UV-Light Driven Photodegradation of Aqueous Organic Pollutants

Ettireddy P. Reddy, Bo Sun, and Panagiotis G. Smirniotis*

Department of Chemical and Materials Engineering, University of Cincinnati, Cincinnati, Ohio 45221-0171

Received: June 15, 2004; In Final Form: August 16, 2004

A number of transition metal (Cr, V, Fe, Cu, Mn, Co, Ni, Mo, and La) incorporated MCM-41 mesoporous molecular sieves with Si/Me = 80 have been synthesized by a hydrothermal method. It was demonstrated that the presence of transition metal salts in the gel during synthesis hinders the action of the template, which results in pores of MCM-41 that are not well-formed. These materials were then loaded with TiO_2 via the sol−gel method, and the resulting materials were explored for the destruction of 4-chlorophenol in the presence of visible, as well as UV, light. A combination of various physicochemical techniques such as N_2 physisorption, O_2 chemisorption, X-ray diffraction (XRD), diffuse reflectance UV−vis (DR UV−vis), and temperature program reduction (TPR) were used to characterize the chemical environment of these transition metals in the prepared catalysts. The dispersion of transition metals as determined by O_2 chemisorption suggests that they are well dispersed inside the MCM-41 framework, but the dispersion values decrease with the loading of TiO_2. This indicates that the loaded titania promotes the transformation of incorporated metal ions into different phases. The UV−vis spectroscopy results of TM-MCM-41 (where TM = Cr, V, Fe, Cu, Mn, Co, Ni, Mo, and La) showed enhancement of light absorption in the visible range by some composite materials. The same materials loaded with titania show higher absorption in the UV range (250−400 nm) due to the presence of titania. Among all TM-MCM-41 materials, only Cr- and Cu-MCM-41 showed strong reduction transitions at lower temperatures; all other TM-MCM-41 materials showed very broad reduction transitions. Titania-loaded Cr-MCM-41 showed an interesting reduction transition at 321 °C due to $Cr^{6+} \rightarrow Cr^{5+}$. This transition was obtained as a result of the strong interaction of Cr−O−Ti inside the MCM-41. The photocatalytic activity under visible and UV light for the degradation of aqueous 4-chlorophenol was tested. Among all of the catalysts, only 25% TiO_2/Cr-MCM-41 exhibited significant activity in visible light. Other 25% TiO_2/TM-MCM-41 samples demonstrated low or no activity to operate with visible light. In contrast, the activities of all 25% TiO_2/TM-MCM-41 catalysts under UV light were found to be more comparable with each other. Their catalytic performances are correlated with the UV−vis spectrum of each synthesized catalyst to reveal the specific role played by each metal ion.

Introduction

Photocatalytic treatment of polluted water and gas has gained increased attention recently.[1,2] It involves the utilization of ultraviolet or solar light by a semiconductor photocatalyst. This technique has been proven successful for the abatement of several different classes of pollutants[3] and even inorganic ions.[4,5] However, the problem of low energy efficiency of the photocatalytic process has hindered its practical application.

Titanium dioxide in the form of anatase is the most stable and most studied photocatalyst. A number of approaches have been followed to enhance the reaction rates of this material. Nanosize titania was able to expose more surface to light and reactants.[6,7] However, smaller particle sizes enhance light scattering,[8] leading to a reduced utilization of light. The incorporation of transition metal ions into TiO_2 is deleterious for photooxidation;[9] it is advantageous only for reduction.[10] The use of CdS as a photocatalyst allows the utilization of visible light, but leads to photocorrosion.[11]

The use of supported titanium dioxide has allowed the enhancement of photodegradation rates in comparison with neat titania.[9,12,13] In particular, Herrmann et al.[9] prepared a composite TiO_2/active carbon catalyst, and Xu and Langford[12,13] combined titania with zeolites and molecular sieves. It was shown that such arrangements (highly adsorptive support and nanosize titania) produced higher quantum yields. The latter research group also attempted to use a transition metal modified MCM-41 support for the composite but found that the effect of the incorporated metal is deleterious.

In the present study, different transition metals were incorporated in the MCM-41 during synthesis. After synthesis, these materials were loaded with titania. All of the materials were characterized by various physicochemical techniques. The activity of TiO_2/TM-MCM-41 catalysts for the degradation of 4-chlorophenol was compared in the presence of UV and/or visible light. Although it has been shown that some metals are indeed deleterious, others can enhance the performance of photocatalysts and even enable them to utilize visible light.

Experimental Section

Synthesis of TiO_2-Loaded Transition Metal Modified MCM-41 Specimens. The transition metal modified MCM-41 specimens were prepared as reported elsewhere.[14] The precursors of the transition metals were $VO(C_3H_7O)_3$ (vanadium), $CrCl_3 \cdot 6H_2O$ (chromium), $MnC_2H_3O_2 \cdot 4H_2O$ (manganese), $Fe_2(SO_4)_3 \cdot$

* Corresponding author. E-mail: Panagiotis.Smirniotis@UC.EDU. Phone: (513) 556 1474, Fax: (513) 556 3473.

10.1021/jp047419m CCC: $27.50
Published on Web 10/08/2004

$7H_2O$ (iron), $Co(NO_3)_2 \cdot 6H_2O$ (cobalt), $Ni(NO_3)_2$ (nickel), $Cu(NO_3)_2 \cdot 2H_2O$ (copper), $(NH_4)_2MoO_3$ (molybdenum), and $LaCl_3$ (lanthanum). All reagents were purchased from Fisher except $LaCl_3$, which was purchased from Aldrich. The atomic ratio of each metal to silica was 1:80 during the synthesis. In a typical preparation procedure, 35 mL of Ludox HS-40 colloidal silica (40%) was added to 14.6 mL of water under stirring, and then, 18.2 mL of 40% tetramethylammonium hydroxide (Fluka) was added. Independently, 18.25 g of cetyltrimethylammonium bromide (CTABr, Alfa Aesar) was dissolved in 33 mL of water, and subsequently, 7 mL of 28% NH_4OH was introduced. Finally, these two solutions were mixed. The corresponding amount of each transition-metal oxide precursor was dissolved in water and added dropwise to the resulting mixture. The final mixture was stirred for 30 min and then transferred into a Teflon bottle and treated under autogenous pressure without stirring at 100 °C for 3 days. The resulting slurry was filtered, washed, dried, and calcined at 550 °C for 10 h with airflow and a heating rate of 2 °C/min.

The resulting catalyst (typically 1.5 g) was dispersed in 100 mL of 2-propanol, and titanium isopropoxide was added to achieve 25% TiO_2 loading. The materials were dried while stirring at ambient temperature and then placed in an oven to dry at 100 °C for 1 h. All photocatalysts were calcined at 450 °C for 3 h with a temperature ramp of 2 °C/min.

Characterization. *BET Surface Area and Pore Size Distribution Measurements*. The specific surface area (BET) and Horvath−Kawazoe pore volume and pore size measurements of the TM-MCM-41 and TiO_2/TM-MCM-41 samples were measured by nitrogen adsorption at 77 K with a Micromeritics ASAP 2010. All samples were degassed at 300 °C under vacuum before analysis.

Oxygen Chemisorption. The dispersion of transition metal in the TM-MCM-41 and TiO_2/TM-MCM-41 samples was determined by oxygen uptake measurements on a Micromeritics Autochemi 2910 system. These measurements were performed in pulse mode using He as the carrier gas (30 STP cm^3/min). The catalysts were prereduced in a continuous flow of 20 mL/min pure H_2 (Matheson) at 370 °C for 2 h. Subsequently, pulses of oxygen (1 mL loop volume, 4 vol %, balance He) were injected into the carrier gas until saturation of the sample was attained. The oxygen uptake was quantified by a temperature control detector (TCD), which was built into the Micromeritics Autochemi 2910 unit. The dispersion of transition metal was expressed as the ratio between the oxygen uptake and the transition metal content, and it was calculated by assuming a stoichiometric factor of oxygen atom to transition metal equal to one (O/TM = 1).

XRD Characterization. XRD was used to identify the crystal phases and structures of the TM-MCM-41 and TiO_2/TM-MCM-41 samples. These studies were performed by using a Nicolet powder X-ray diffractometer equipped with a Cu Kα radiation source (wavelength 1.5406 Å). An aluminum holder was used to support the catalyst samples. All of the powder samples were run from 2° to 7° (2θ) with a step size of 0.01° and a time step of 1.0 s to assess the structure of the matrix. TiO_2/TM-MCM-41 samples were also run from 20° to 50° with a step size of 0.05° and a time step of 1.0 s to assess the crystallinity of the TiO_2 loading.

UV−Vis Characterization. The powders were characterized by a UV−vis spectrophotometer (Shimadzu 2501PC) equipped with an integrating sphere attachment ISR1200 for their diffuse reflectance, and the range of wavelengths employed was 200−900 nm. $BaSO_4$ was used as the standard in these measurements.

Temperature Program Reduction (TPR). TPR experiments were carried out on a Micromeritics Autochemi 2910. Approximately 100 mg of sample was put in a quartz U tube and packed with quartz wool below and above the sample. Then, this U tube was fixed to the analyzer port of the Autochemi 2910 system. The sample was pretreated with a continuous flow of 20 mL/min ultrahigh-purity oxygen (Matheson) at 200 °C for 2 h. The reducing gas, a mixture of 10 vol % H_2 in Ar (Matheson), at a flow rate of 20 mL/min, was used to test the sample with the temperature increasing from 50 to 550 °C at a rate of 2 °C/min. The amount of hydrogen consumed by the sample in a given temperature range (in μmol/g) was calculated by integrating the TCD signal intensities under the corresponding TCD peaks.

Catalytic Activity. *UV and Visible Light Photocatalytic Performance Experiments.* The photocatalytic testing included the degradation of 4-chlorophenol, which was performed in a round, flat-plate, batch reactor used somewhere else.[14] A 450-W medium-pressure mercury lamp (Jelight) was employed as the light source to conduct UV−visible light experiments. A double-acrylic OP-2 (museum quality) sheet was placed between the light source and the reactor for the purpose of excluding UV radiation when we wanted to conduct visible-light experiments. The cooling jacket around the reactor effectively precluded the IR part of the spectrum from penetrating into the reaction solution and cooled the lamp. A 0.5 L aliquot of 1 mM 4-chlorophenol (used as the probe molecule for the photodegradation) in deionized water was ultrasonicated with 0.4 g of catalyst for 10 min in an ultrasonic bath in order to ensure the deagglomeration of catalyst aggregates. The suspended catalyst in aqueous system was oxygenated (Wright Brothers, 99.9%) at 0.5 L/min to ensure complete saturation. The temperature in the reactor was kept constant at 25 ± 1 °C. The pH of the reaction suspension was not adjusted. Samples of the reaction suspension were taken with a syringe at different intervals and filtered with Cameo 25P polypropylene syringe filters (OSMONICS, cat #DDP02T2550). The sample solutions were analyzed with a total rrganic carbon analyzer (TOC−VCSH, Shimadzu).

Results and Discussion

Sensitization of titania was found to be an efficient way to enhance the performance of solar cells[15] by the expansion of their working range into visible light. To achieve a similar effect for the photodegradation of aqueous organics, one needs to use an inorganic sensitizer to avoid self-degradation of the catalyst. Our group[14,16] proposed using transition metal incorporated MCM-41 supports as such sensitizers for TiO_2. Summarized herewith are the characterization and photocatalytic results for the photocatalysts incorporated with various transition metal ions.

The major surface characterization results of these materials are summarized in Tables 1 and 2. One can observe that the presence of transition metal ions in the gel during synthesis lowers the surface area (SA) of the resulting MCM-41 materials (for example, SA = 1105 m^2/g for siliceous MCM-41, and SA = 991 m^2/g for Cr-MCM-41). The pore size also changes with the introduction of the transition metal. Because the same surfactant template was utilized for the synthesis of both siliceous and transition metal incorporated MCM-41 materials, the pore sizes of both materials are expected to be in a close range. The presence of transition metal salts changes the ionic strength of the gel during synthesis, which may hinder the action of the template and result in the formation of partially broken

TABLE 1: Characterization Results for Transition Metal Incorporated MCM-41 Materials Utilized in the Present Study

TM-MCM-41	BET SA (m^2/g)	pore volume (cm^3/g)	peak pore size (nm)	O_2 chemisorption (μmol/g catalyst)	metal dispersion[a] (%)	site density (10^{14} atoms /m^2 surface)	active particle diameter (nm)
MCM-41	1105	1.10	3.8				
Cr-MCM-41	991	0.89	3.5	34.53	16.79	210.00	6.7
Fe-MCM-41	1064	1.27	4.6	2.68	1.29	15.20	89.2
V-MCM-41	1103	1.10	3.8	0.67	0.32	3.65	377.7
Cu-MCM-41	941	1.31	5.4	57.95	27.11	371.00	3.7
Mn-MCM-41	1048	1.00	3.7	0.62	0.30	3.59	336.9
Co-MCM-41	947	1.56	6.4	1.78	0.88	11.40	113.6
Ni-MCM-41	1015	1.56	6.0	2.32	1.12	13.80	90.8
La-MCM-41	853	1.55	7.0	0.04	0.01	0.36	16 529.7
Mo-MCM-41	1096	1.18	4.2	0.98	0.47	5.39	270.4

[a] Metal dispersion was determined from oxygen chemisorption measurements by using a stoichiometric factor of metal to oxygen equal to 1.

TABLE 2: Characterization Results for Titania-Loaded Transition Metal Incorporated MCM-41 Materials Utilized in the Present Study

25% TiO_2-loaded TM-MCM-41	BET SA (m^2/g)	pore volume (cm^3/g)	peak pore size (nm)	O_2 chemisorption (μmol/g catalyst)	metal dispersion[a] (%)	site density (10^{14} atom/ m^2 surface)	active particle diameter (nm)
25%TiO_2/MCM-41	879	0.78	3.4				
25%TiO_2/Cr-MCM-41	740	0.71	3.7	0.89	0.59	7.26	193.4
25% TiO_2/Fe-MCM-41	753	0.78	4.0	1.96	1.27	15.70	90.6
25% TiO_2/V-MCM-41	852	0.71	3.2	0.09	0.05	0.63	2288.6
25%TiO_2/Cu-MCM-41	753	0.93	4.8	9.90	6.41	79.20	16.3
25%TiO_2/Mn-MCM-41	916	0.86	3.6	2.81	1.81	18.50	56.7
25%TiO_2/Co-MCM-41	711	0.96	5.3	0.71	0.46	6.05	218.8
25%TiO_2/Ni-MCM-41	703	0.90	5.0	0.31	0.20	2.68	503.3
25%TiO_2/La-MCM-41	708	1.07	5.9	1.03	0.65	8.73	289.2
25%TiO_2/Mo-MCM-41	867	0.84	3.8	0.18	0.10	1.24	1256.9

[a] Metal dispersion was determined from oxygen chemisorption measurements by using a stoichiometric factor of metal to oxygen equal to 1.

pores as well as a lower SA. The latter phenomenon was also supported by the XRD results to be discussed below. The size of the metal ions for incorporation can also affect the pore formation during synthesis and, in turn, influence the pore quality. Moreover, some loss of SA is observed when titania is deposited on the MCM-41 support. The pore size of MCM-41 also decreases with the loading of titania as expected. This is a logical conclusion of the loss of surface area caused by partial blockage of the pores.

One of the best ways to characterize transition metal incorporated MCM-41 materials is to determine the dispersion of transition metal inside the MCM-41 framework. The commonly accepted method is selective chemisorption of a suitable gas such as oxygen. The choice of the temperature at which oxygen chemisorption could give meaningful information about the dispersion of transition metal inside MCM-41 was deemed crucial. Oyama et al.[17] have proposed that if the temperature of oxygen chemisorption of silica-supported vanadia catalysts is around 370 °C with a prereduction of the catalysts at the same temperature, the results would give much more meaningful information than the results generated at a low temperature with sample prereduction above 500 °C. Reddy et al.[18] have reported that the oxygen chemisorption of titania-supported vanadia catalysts measured at 370 °C with sample prereduction at the same temperature probably avoids bulk and/or over-reduction of vanadium oxide and sintering of the support materials. For comparison purposes, we have measured the oxygen pulse chemisorption at 370 °C for all TM-MCM-41 and TiO_2/TM-MCM-41, which were prereduced at an identical temperature.

Oxygen uptake values obtained at 370 °C for various TM-MCM-41 are presented in Table 1. The siliceous MCM-41 did not chemisorb any oxygen at the selected experimental conditions. Therefore, the oxygen chemisorption contribution of siliceous MCM-41 is zero for all TM-MCM-41 materials. As shown in Table 1, the greatest oxygen chemisorption was observed for copper- and chromium-incorporated samples, followed by iron-, nickel-, cobalt-, molybdenum-, vanadium-, manganese-, and lanthanum-incorporated ones. This phenomenon can be explained by the highly reduced form of Cr and Cu during the prereduction and the unreduced forms of other transition metals in the MCM-41 framework; the same trend was also observed in the TPR study (see later paragraphs). The metal dispersion was estimated from the oxygen chemisorption by using the stoichiometric factor of oxygen-atom-to-metal equal to one (O/TM = 1). The dispersion is defined as the percentage of metal oxide units available for reduction and subsequent oxygen uptake. It is estimated from the total number of metal oxide units present in the sample and the number of oxygen atoms chemisorbed. As shown in Table 1, Cr-MCM-41 and Cu-MCM-41 have high metal dispersion values. Even though the dispersion of Cu in Cu-MCM-41 is higher than that of Cr in Cr-MCM-41, the photocatalytic activity of TiO_2/Cr-MCM-41 under visible light is significantly higher than that of TiO_2/Cu-MCM-41, as will be discussed below. The oxygen atom site density as a function of transition metal incorporated in MCM-41 is summarized in Table 1. The active sites of transition metal incorporated in MCM-41 are imagined as vacancies created by the removal of labile oxygen atoms that take part in the redox processes in the oxidation or photooxidation reactions. The values of oxygen atom site density of Cr- and Cu-MCM-41 samples obtained from oxygen chemisorption are drastically higher than values from the other transition metal incorporated MCM-41 materials. The average particle diameters of TM-MCM-41 materials determined during the oxygen

chemisorption measurements are listed in Table 1. The average particle diameter of La-MCM-41 is approximately 10 times higher than that of other TM-MCM-41 materials, and thus, it suggests that La may not be incorporated properly inside the MCM-41 matrix because of its relatively large ionic diameter. Cu-MCM-41 and Cr-MCM-41 materials have very low particle size, which indicates that the Cu and Cr are incorporated in a very orderly manner, as compared to others inside the framework of MCM-41. These results are in perfect agreement with the TPR results to be described in the later paragraphs.

The oxygen chemisorption, metal dispersion, oxygen atom site density, and average particle diameter of titania-loaded TM-MCM-41 materials were summarized in Table 2. The oxygen chemisoprtion values of TM-MCM-41, except Mn-MCM-41 and La-MCM-41, materials decreased significantly after titania loading. This decrease in the oxygen uptake values is very high in the case of titania-loaded Cr-MCM-41, which is followed by Ni-, V-, Cu-, Mo-, Co-, and Fe-MCM-41 materials. This indicates that the surface-exposed oxygen inside Cr-MCM-41 was strongly interacting with titania. Because of this strong Cr−Ti interaction, the loaded titania is uniformly distributed throughout the Cr-MCM-41. This is the reason the active particle diameter of 25% TiO_2/Cr-MCM-41 is significantly higher than that of Cr-MCM-41. The values of oxygen uptake, metal dispersion, site density, and active particle diameter of 25% TiO_2/Fe-MCM-41 are almost the same as those of Fe-MCM-41, which demonstrates that there is no strong interaction between Fe and titania. Thus, the BET surface area, pore volume, and pore size of the Fe-MCM-41 decrease after titania loading. Oxygen chemisorption, metal dispersion, and site density values of V-, Cu-, Co-, Ni-, and Mo-MCM-41 decreased more than three times after loading titania on these materials. The active particle diameter of these materials increased accordingly. This clearly suggests there can be a strong interaction between the transition metal and titania inside the matrix of MCM-41, which makes it more difficult for the transition metal to be reduced than in TM-MCM-41. The 25% TiO_2/Mn-MCM-41 material shows four times higher oxygen uptake values than Mn-MCM-41, probably because of the higher redox property of the Mn−O−Ti species in comparison to the Mn−O−Si of Mn-MCM-41. The same trend, but significantly higher (25 times higher than La-MCM-41) values, was observed for titania-loaded La-MCM-41 than for the corresponding MCM-41 material. The oxygen uptake values of 25% TiO_2/TM-MCM-41, except 25% TiO_2/Cu-MCM-41, are very low, because these transition metals are unable to reoxidize in the oxygen uptake experiments.

XRD patterns can allow the assessment of the matrix structures of the catalysts. Figures 1−2 show the XRD patterns of TM-MCM-41 before and after loading of the TiO_2. One can observe that the incorporation of transition metal into MCM-41 hinders the formation of the tubular mesoporous structure as shown by the intensities of the main peak ($2\theta \approx 2.5°$) that are approximately 20% lower than that of pure siliceous MCM-41. The XRD reflections 100, 110, and 200 of the TM-MCM-41 are determined to be almost at the same locations as those of siliceous MCM-41,[1,2] whereas the XRD reflections of titania-loaded TM-MCM-41 (where TM = V, Cr, Mn, Fe, Co, Ni, Cu, Mo, and La) are lower than those of the TM-MCM-41 and siliceous MCM-41. The positions of the XRD reflections for TM-MCM-41 and 25% TiO_2/TM-MCM-41 are indexed to a hexagonal lattice structure. The intensities of these peaks of TM-MCM-41 are lower when compared to the MCM-41. This suggests that the presence of transition metal ions obstructs the structure-directing action of the template by changing its ionic strength.[14] One more interesting point is that we could not detect any peaks associated with transition metals or transition metal oxides. This indicates that the transition metal ions are incorporated into the MCM-41 framework. As shown in Figure 1, the d_{100} and unit-cell parameters of TM-MCM-41 are very close to those of the siliceous MCM-41, which demonstrates that the MCM-41 structure is slightly modified by the transition metals incorporated in the MCM-41 framework. Gratzel[15] also reported that tungsten was incorporated in the MCM-41 framework even though the radius of the tungsten ion is larger than the radii of transition metal ions used in our study.

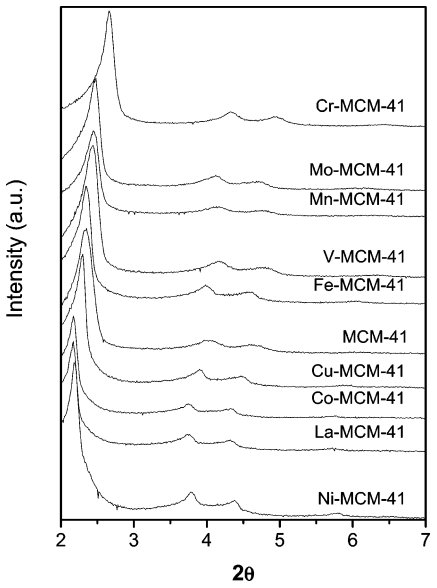

Figure 1. XRD diffractograms of transition metal (V, Cr, Fe, Cu, Mn, Co, Ni, La, Mo) incorporated MCM-41 (Si/Me = 80) materials.

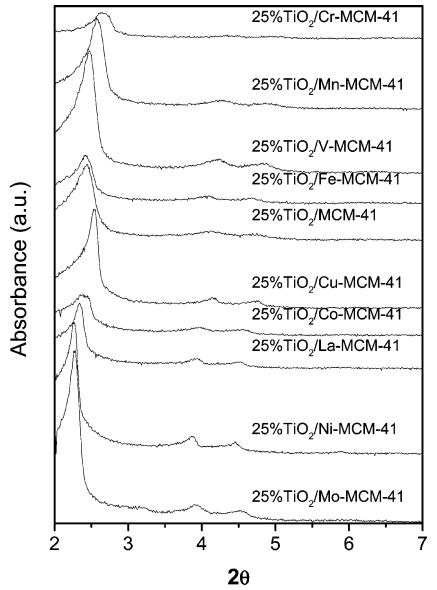

Figure 2. XRD diffractograms of 25% TiO_2-loaded transition metal incorporated MCM-41 materials.

The XRD analysis of the composite catalysts in the range 20−50° (not shown) demonstrated that the titania loaded according to the procedure used in the study is in amorphous form. The latter property may enable one to use the approach of Kisch et al.,[19] who sensitized amorphous titania with noble-metal halogenides to achieve the performance in visible light.

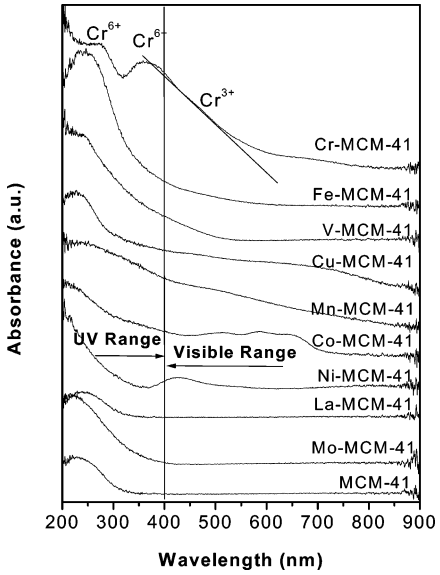

Figure 3. UV−vis diffuse reflectance spectra of the transition metal incorporated MCM-41 supports.

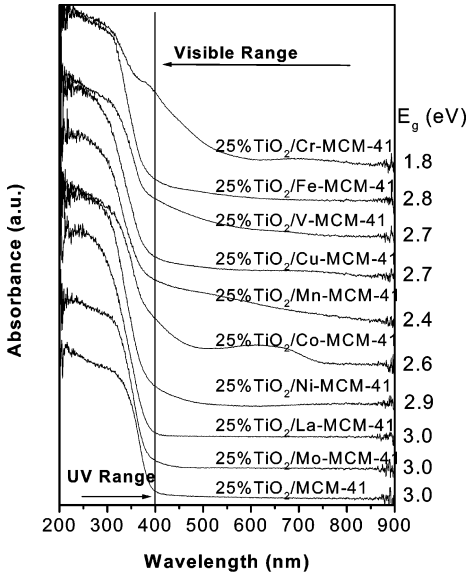

Figure 4. UV−vis diffuse reflectance spectra of the titania-loaded transition metal incorporated photocatalysts (titania loading 25 wt %).

To ascertain the capability of each particular composite material to photodegrade organic chemicals in the visible range of spectrum, one needs to analyze the UV−vis diffuse reflectance spectra (Figures 3−4). This allows us to observe the absorption in the UV and visible parts of the spectrum by the dispersed transition metal oxides in the framework (Figure 3). In particular, the absorption peak at 375 nm corresponds to Cr^{6+} and that at 450 nm to Cr^{3+}. For vanadium-incorporated material, only the peak at 575 nm is observed, which corresponds to V^{5+} species. Iron in Fe-MCM-41 exists as only a +3 oxidation state, as demonstrated by the absorption peak at 250 nm. One peak is shown at 423 nm for nickel-incorporated MCM-41, which belongs to Ni^{2+}. The peak for Co-MCM-41 is at 600 nm, belonging to Co^{2+}. There is no peak for La-MCM-41. No definite peak can be identified in the spectrum curve for Cu-MCM-41, so Cu exists as Cu^{+} and Cu^{2+}. The peak on the Mn-MCM-41 spectrum curve is around 375 nm. When considering titania-loaded materials (Figure 4), one can observe significant absorption in the UV range due to the presence of titania. Nonetheless, the absorption spectra of the TiO_2-loaded samples

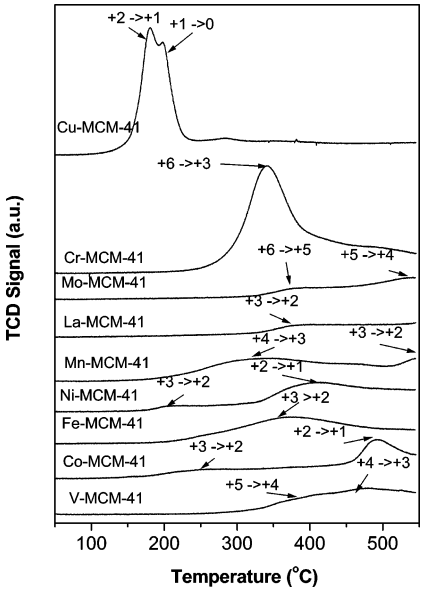

Figure 5. TPR profiles of transiton metal incorporated MCM-41 (Si/Me = 80) (reduction temperature range 50−550 °C).

TABLE 3: TPR Reduction Transitions of TM-MCM-41 Materials Obtained at Different Temperatures

	TPR reduction transitions		total H_2 consumption (μ mol/g of catalysts)
TM-MCM-41	peak 1 (°C)	peak 2 (°C)	
Cu-MCM-41	181 (Cu^{2+} to Cu^{1+})	201 (Cu^{1+} to Cu^{0})	192.4
Cr-MCM-41	343 (Cr^{6+} to Cr^{3+})	490 (Cr^{3+} to Cr^{2+})	257.1
Mo-MCM-41	379 (Mo^{6+} to Mo^{5+})	545 (Mo^{5+} to Mo^{4+})	13.9
La-MCM-41	389 (La^{3+} to La^{2+})		20.3
Mn-MCM-41	318 (Mn^{4+} to Mn^{3+})	550 (Mn^{3+} to Mn^{2+})	92.0
Ni-MCM-41	211 (Ni^{2+} to Ni^{+})	410 (Ni^{+} to Ni^{0})	69.6
Fe-MCM-41	372 (Fe^{3+} to Fe^{2+})		106.7
Co-MCM-41	251 (Co^{3+} to Co^{2+})	490 (Co^{2+} to Co^{1+})	54.3
V-MCM-41	398 (V^{+5} to V^{+4})	481 (V^{+4} to V^{+3})	156.7

shown in Figure 4 are different from those of neat titania (not shown). Absorption shoulders typical of loaded titania are observed for the chromium- and iron-incorporated materials.[20] However, the spectrum of vanadium-incorporated material is smooth. Conclusively, the UV−vis study shows the coexistence of two valence states of chromium and elucidates the absence of the doping effects in La-incorporated samples.

TPR was used to investigate different oxidation states of the TM-MCM-41 materials in the reduction temperature range 50−550 °C. No TPR study was done at elevated temperature in order to maintain the MCM-41 structure. TPR profiles for all TM-MCM-41 materials are illustrated in Figure 5. The total hydrogen consumption and reduction temperature for TM-MCM-41 are expressed in Table 3. One can observe that the reduction behavior of each transition metal incorporated MCM-41 was quite different from the others. As shown in Figure 5, the TPR profiles of most of the transition metal incorporated MCM-41 materials showed more than one reduction transition peaks. These peaks are not clearly separated because of differences caused by metal dispersion, particle size, and the interaction between MCM-41 and the metal oxide species. Figure 5 showed that only one reduction peak at approximately 190 °C was observed for Cu-MCM-41. This peak was split into two peaks, one at 181 °C and the other at 203 °C, which is probably due to the similar reduction properties of Cu^{2+} and Cu^{+} in the MCM-41 matrix. The first peak at 181 °C corresponds to the reduction of $Cu^{2+} \rightarrow Cu^{+}$, and the second peak at 203 °C is due to the reduction of $Cu^{+} \rightarrow Cu^{0}$. This

TABLE 4: TPR Reduction Transitions of 25% TiO_2/TM-MCM-41 Materials Obtained at Different Temperatures

25% TiO_2-loaded TM-MCM-41	TPR Reductions Transitions				total H_2 consumption (μ mol/g of catalysts)
	peak 1 (°C)	peak 2 (°C)	peak 3 (°C)	peak 4 (°C)	
Cu-MCM-41	157: interfacial oxygen ion	180 (Cu^{2+} to Cu^{+})	196 (Cu^{+} to Cu^{0})	277 (Ti^{4+} to Ti^{3+})	163.9
Cr-MCM-41	267 (Ti^{4+} to Ti^{3+})	321 (Cr^{6+} to Cr^{5+})	396 (Cr^{5+} to Cr^{3+})	491 (Cr^{3+} to Cr^{2+})	114.7
Mo-MCM-41	364 (Ti^{4+} to Ti^{3+})	419 (Mo^{6+} to Mo^{5+})	497 (Mo^{5+} to Mo^{4+})		29.0
La-MCM-41	381 (Ti^{4+} to Ti^{3+})	503 (La^{3+} to La^{2+})			79.2
Mn-MCM-41	210 (Ti^{4+} to Ti^{3+})	293 (Mn^{4+} to Mn^{3+})	471 (Mn^{3+} to Mn^{2+})		75.5
Ni-MCM-41	301 (Ti^{4+} to Ti^{3+})	343 (Ni^{3+} to Ni^{2+})	444 (Ni^{2+} to Ni^{+})		113.6
Fe-MCM-41	271 (Ti^{4+} to Ti^{3+})	299 (Fe^{3+} to Fe^{2+})	371 (Fe^{2+} to Fe^{0})		94.6
Co-MCM-41	220 (Ti^{4+} to Ti^{3+})	286 (Co^{3+} to Co^{2+})	390 (Co^{2+} to Co^{+})		24.9
V-MCM-41	344 (Ti^{4+} to Ti^{3+})	392 (V^{5+} to V^{4+})	467 (V^{4+} to V^{3+})		69.2

result clearly indicates that the Cu is incorporated as Cu^{2+} inside the MCM-41 framework. Moreover, the total volume of hydrogen consumed for the reduction of Cu-MCM-41 is exactly equivalent to that needed for the reduction of Cu^{2+} to Cu^{0} per gram of Cu-MCM-41. In the case of Cr-MCM-41 (see Figure 5), one can observe that there is only one major peak at 343 °C and one shoulder peak at 490 °C. The major peak at 343 °C corresponds to the reduction of $Cr^{6+} \rightarrow Cr^{3+}$, and the shoulder peak at 490 °C may be due to the partial reduction of $Cr^{3+} \rightarrow Cr^{2+}$. The average oxidation state of Cr in Cr-MCM-41 is equal to 5.81, as calculated from the total volume of hydrogen adsorption in the TPR experiment. The TPR peaks of Mo-MCM-41 at 419 and 545 °C can be considered as the reductions of $Mo^{6+} \rightarrow Mo^{5+}$ and $Mo^{5+} \rightarrow Mo^{4+}$, respectively. The total H_2 volume adsorbed in Mo-MCM-41 is much less compared to that in Cu- and Cr-MCM-41 and may due to a lower amount of the Mo^{6+} state dispersed in the framework. The TPR profile of La-MCM-41 shows only one small reduction peak at 389 °C, which possibly corresponds to the transition of $La^{3+} \rightarrow La^{2+}$ in dispersed lanthanum oxide. As explained in the oxygen uptake results, the active particle diameter of La-MCM-41 is very large; this may be due to a large amount of bulk La_2O_3, which was present instead of dispersed La inside the MCM-41 matrix. As reported in the literature, the bulk La_2O_3 reduces at approximately 700 °C.[21] As shown in Figure 5, the TPR profile of Mn-MCM-41 showed a two-step reduction. The first reduction at 318 °C corresponds to the $Mn^{4+} \rightarrow Mn^{3+}$ transition, and the second reduction at 550 °C is due to the $Mn^{3+} \rightarrow Mn^{2+}$ transition. Ni-MCM-41 also exhibits a two-step reduction, which can be explained as a result of the slow reduction of some NiO weakly bound to the silica surface of MCM-41.[22] This weakly bound NiO reduced as two reduction transitions at 211 and 410 °C, which are associated to $Ni^{2+} \rightarrow Ni^{+}$ and $Ni^{+} \rightarrow Ni^{0}$, respectively. In the case of Fe-MCM-41, the reduction proceeds in the range 220−450 °C, and the reduction transition is recorded at 372 °C; this phenomenon was mainly assigned to the fraction of readily reducible ($Fe^{3+} \rightarrow Fe^{2+}$) iron oxide particles. Two different reduction peaks have been observed for Co-MCM-41, which indicates the existence of differently reducible cobalt species in the MCM-41. Reduction of cobalt species ($Co^{3+} \rightarrow Co^{2+}$) at temperatures higher than 500 °C indicates the strong interaction of cobalt with the surface. In contrast, the reducibility at a lower temperature (251 °C) than that of bulk cobalt oxide is due to the particle size of the cobalt oxide and the electronic interaction between the cobalt and the MCM-41. The TPR profile of V-MCM-41 shows only one broad reduction transition ($V^{5+} \rightarrow V^{3+}$) at approximately 500 °C. Wachs and co-workers[23] have reported that the reduction peak of surface vanadium oxide highly dispersed on silica appears at 525 °C. This temperature is almost the same as that observed here for V-MCM-41. This clearly indicates that the coordination environment of the vanadium species in V-MCM-41 resembles highly dispersed vanadium oxide on the silica.

The TPR profiles of titania-loaded TM-MCM-41 materials are presented in Figure 6. The reduction transitions and total

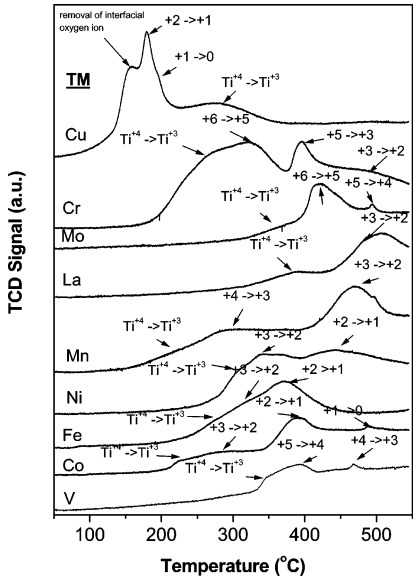

Figure 6. TPR profiles of 25% TiO_2-loaded transition metal incorporated MCM-41 materials (reduction temperature range 50−550 °C).

volume of H_2 adsorption for these materials are summarized in Table 4. One can observe from Figure 6 that TiO_2/TM-MCM-41 materials can be reduced at lower temperatures when compared to the corresponding TM-MCM-41 materials. This clearly indicates that there is a strong interaction between metal and TiO_2 in TiO_2/TM-MCM-41 through Ti−O−TM, which can be reduced at a lower temperature than Si−O−TM in the corresponding TM-MCM-41. Deo and Wachs[24] have reported that vanadium oxide bridge-bonded with ZrO_2 (Zr−O−V) is more reducible than that with terminal-bonded oxygen (V═O). The broad shoulder peak in the range 250−380 °C corresponds to the dehydroxylation of the TiO_2 surface and also the reduction of titania from +4 to +3.[25] This peak is observed in all TiO_2/TM-MCM-41 TPR profiles (Figure 6). The TPR profile of TiO_2/Cu-MCM-41 shows a remarkable difference from that of Cu-MCM-41. Four reduction peaks (157, 180, 196, and 277 °C) were observed in the case of TiO_2/Cu-MCM-41. The positions of the peaks shift to lower temperatures in comparison with those for Cu-MCM-41. The lowering of the reduction temperature can be attributed to the interaction of Cu and TiO_2. The peaks at 180 and 196 °C correspond to the reductions of $Cu^{2+} \rightarrow Cu^{+}$ and $Cu^{+} \rightarrow Cu^{0}$, respectively. Dow and Huang[26] have reported that, when CuO is supported on YSZ (Y_2O_3-stabilized

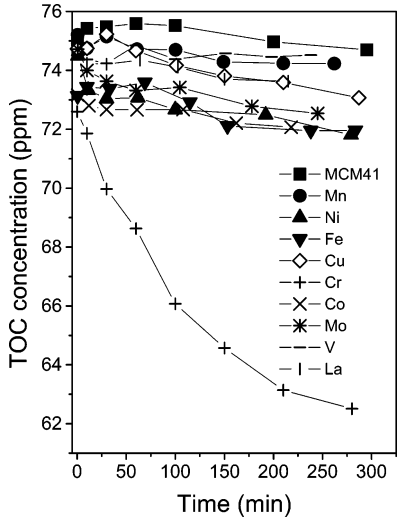

Figure 7. Time course of total carbon concentration in 4-chlorophenol photodegradation using UV light. Initial 4-chlorophenol concentration, 1 mM; temperature, 25 ± 1 °C.

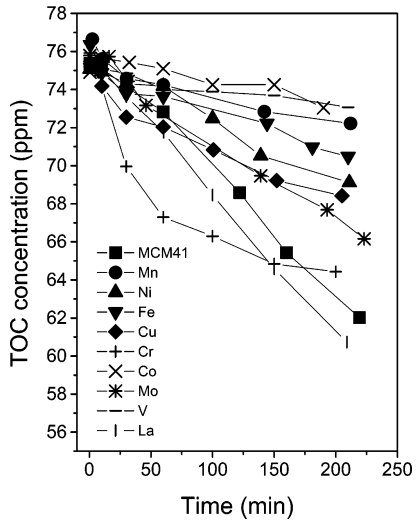

Figure 8. Time course of total carbon concentration in 4-chlorophenol photodegradation using visible light. Initial 4-chlorophenol concentration, 1 mM; temperature, 25 ± 1 °C.

ZrO_2), the interfacial oxygen ion of copper oxide can be removed at a very low temperature (157 °C). The reduction temperatures of TiO_2/Cr-MCM-41 are completely different than those of Cr-MCM-41. This can be due to the strong interaction between Cr and TiO_2 (Cr−O−Ti) inside the MCM-41. As explained earlier in this paragraph, the first peak at 267 °C is due to the partial hydroxylation and reduction of TiO_2. In addition to the reduction transitions of Cr-MCM-41, the 25% TiO_2/Cr-MCM-41 shows a new reduction transition at 321 °C attributed to $Cr^{6+} \rightarrow Cr^{5+}$, which is made possible by the interaction between Cr and TiO_2. The interaction is the main reason that 25% TiO_2/Cr-MCM-41 is an active photocatalyst in visible light. All other TiO_2/TM-MCM-41 catalysts also show remarkably different reduction transitions from those of the corresponding TM-MCM-41 (Tables 3−4). TPR results of these TiO_2/TM-MCM-41 catalysts show that the interaction of titania with transition metal is different in each catalyst. Kevan et al.[25] have reported that the reduction transition depends on the conditions applied during the TPR experiments, such as the concentration and partial pressure of hydrogen and heating rate. Moreover, the reduction transitions also depend on the metal dispersion, particle size, and the interaction between TiO_2 and the transition metal incorporated inside MCM-41. Therefore, it is difficult to discuss the reduction temperature differences from the data obtained under the different conditions reported in the literature. The reported reduction transitions are quite different, even for the same materials in the literature.

On the basis of the surface characterization results described earlier, it is now instructive to compare the photocatalytic activities of all TiO_2/TM-MCM-41 materials. Figure 7 shows the total organic carbon (TOC) concentration curves of 4-chlorophenol degradation over 25% TiO_2/TM-MCM-41 with the corresponding time courses under visible light. We can see that Cr-incorporated catalyst is much more active than the other transition metal incorporated MCM-41 catalysts. This catalyst deactivated after 280 min in the visible light. The deactivation mechanism was proposed to be the gradual reduction of Cr^{6+}.[14] The catalyst showing no deactivation usually photooxidized organic compounds in a linear relationship with time, because the amount of active oxygen species for oxidation[27] was kept constant during photooxidation. Here, it was assumed that the amount of activation sites decreased proportionally with the active Cr sites left (A_{AC})

$$-\frac{dA_{AC}}{dt} = k_1 A_{AC} \tag{1}$$

The total carbon decomposition rate should be proportional to the concentration of oxygen species in the solution, which in turn is proportional to the amount of the active Cr sites A_{AC} left in the catalysts

$$-\frac{dC}{dt} = k_2 A_{AC} \tag{2}$$

Integration of these two differential equations gave

$$C = \frac{k_2 A_{AC,0}}{k_1} e^{-k_1 t} + \left(C_0 - \frac{k_2 A_{AC,0}}{k_1}\right) \tag{3}$$

in which $A_{AC,0}$ was the initial active Cr sites, k_1 and k_2 were constants, and C_0 was the TOC concentration at $t = 0$. The equation was used for correlation of the experimental curves, and they fit well. The results were $k_1 = 0.0082 \pm 0.0008$/min, $k_2 A_{AC,0} = 0.093 \pm 0.009$ mg carbon/(L·min), which was the initial total carbon decomposition rate.

Visible light provides enough energy for the electrons to leap from valence band to conduction band, and Cr^{6+} acts as an intermediate level for electron excitation under visible light. It is based on the sensitization of titania with a tetrahedrally coordinated transition metal oxide, which can scavenge electrons from the valence band and release electrons to the conduction band upon excitation by visible light, thus bringing about charge separation. The charges can then react with the adsorbed oxygen and surface hydroxyl groups, producing reactive oxygen species. When UV light is utilized, the activity of 25% TiO_2/Cr-MCM-41 becomes slightly higher (Figure 8), simply because more light becomes available. The deactivation of Cr-incorporated catalyst was observed under both UV and visible light photocatalysis, which was caused by the reduction of Cr^{6+} (yellow) to Cr^{3+} (pale green). The interaction of the reduced state of Cr^{3+} and TiO_2 makes the recombination of electrons and holes much easier, so after a certain time, the activity of this catalyst plateaus, even under UV light.

Transition metals other than Cr behave unexpectedly in the composite catalysts utilized in the visible light photodegradation of 4-chlorophenol. Although Mn-, V-, Co-, and Ni-incorporated

TABLE 5: Photocatalytic Activity of the Catalysts Utilized in the Present Study[a]

	reaction rate, mg carbon/(L·min)	
catalyst	UV + visible[b]	visible[c]
25% TiO_2/MCM-41	0.062 ± 0.002	0.004 ± 0.001
25% TiO_2/Cr-MCM-41	0.146 ± 0.025[d]	0.046 ± 0.004[e]
25% TiO_2/Fe-MCM-41	0.024 ± 0.003	0.006 ± 0.001
25% TiO_2/V-MCM-41	0.010 ± 0.002	0.001 ± 0.001
25% TiO_2/Cu-MCM-41	0.032 ± 0.004	0.007 ± 0.002
25% TiO_2/Mn-MCM-41	0.018 ± 0.002	0.004 ± 0.001
25% TiO_2/Co-MCM-41	0.015 ± 0.002	0.004 ± 0.001
25% TiO_2/Ni-MCM-41	0.030 ± 0.002	0.007 ± 0.002
25% TiO_2/La-MCM-41	0.074 ± 0.002	0.005 ± 0.002
25% TiO_2/Mo-MCM-41	0.043 ± 0.002	0.007 ± 0.002

[a] Reactant, 4-chlorophenol; initial concentration, 1 mM; catalyst concentration, 0.8 g/L; temperature = 25 °C. [b] No filter installed. [c] Filter installed. [d] Reaction rate in the first 1 h, after which deactivation is observed. [e] Reaction rate in the first 3 h, after which deactivation is observed.

materials absorb visible light (Figure 4), their photocatalytic activity is negligible under visible light (Figure 7). The inactivity of these catalysts can be explained by their inability to act as an energy level for electrons created in TiO_2 to leap. It can be seen that Mn^{3+} is combined effectively with TiO_2, because its surface metal dispersion was kept high after TiO_2 loading. Mn^{3+}-incorporated catalyst was inactive, because of the small energy driving force for electrons to detrap from Mn^{2+}.[27]

One can observe that the incorporation of certain transition metals (V, Mn, Fe, Co, Ni, and Mo) is, in fact, deleterious for photodegradation under UV light. This is because these metals hindered the photoactivity in UV light exhibited by titania-loaded unmodified MCM-41 and accelerated the electron and hole recombination by acting as intermediate levels.[28] As mentioned already, the interaction of titania-loaded and transition metal ions in our samples creates a plurality of surface defects,[27] which increases the likelihood of recombination of the light-induced charges. Therefore, the activity of TiO_2/TM-MCM-41 (V, Mn, Fe, Co, Ni, and Mo) is low. The comparison for two cases (UV light and visible light) of the degradation of 4-chlorophenol was presented in Table 5 in the form of reaction rates. One can also observe that the activity of titania-loaded Cu-MCM-41 catalyst is higher than that of the Mn-, V-, Fe-, Co-, and Ni-incorporated catalysts under UV light. Furthermore, we found that TiO_2/Cu-MCM-41 is less active than TiO_2/MCM-41. In contrast, Yamashito et al.[29] found increased activity of copper-modified titania in comparison with that of neat titania. They related it to the sensitization effect, wherein the composite catalyst can simply utilize more light. In our case, it is possible that the electron created in titania under the action of UV light reduces copper from +2 into +1 state initially. Cu^+ may act as a recombination center, although Cu_2O may enable the composite to utilize both the visible and UV parts of the spectrum, because Cu_2O itself is capable of water-splitting in visible light.[30]

Conclusions

A number of transition metal incorporated MCM-41 materials were synthesized and loaded with titania. It was demonstrated that the presence of transition metal salt in the gel during synthesis hinders the action of the template and results in pores of MCM-41 that are not well-formed. The characterization results showed enhancement of the absorption in visible light by some composite materials (Cr, Fe, V, Cu, Mn, Co, and Ni). The photocatalytic activity of TiO_2/TM-MCM-41 in visible and/or UV light for the degradation of aqueous 4-chlorophenol was also tested. Only 25% TiO_2/Cr-MCM-41 exhibited considerable activity in visible light. Other TiO_2/TM-MCM-41 materials were not active in visible light. The incorporation of La did not result in any absorption of light in the visible band. Even though the Ni and Co incorporated inside the MCM-41 interacted with TiO_2 during calcinations, both of them cannot bridge the valence and conduction bands of TiO_2 for the electrons to leap with energy less than the band gap. V^{5+}-incorporated catalyst can absorb visible light, but it did not enable the photocatalyst to utilize visible light, as the stability of a close electronic shell also affects the electron trapping as well as its favorable energy level for the electrons to leap. Mn^{3+}-incorporated catalyst was inactive because of the small energy driving force for electrons to detrap from Mn^{2+}.

Acknowledgment. The authors wish to acknowledge the U.S. Department of Army for partial support for this work through the grants DAAD 19-00-1-0399. We also acknowledge funding from the Ohio Board of Regents (OBR) that provided matching funds for equipment to the NSF CTS-9619392 grant through the OBR Action Fund #333.

References and Notes

(1) Peral, J.; Domenech, X.; Ollis, D. F. *J. Chem. Technol. Biotechnol.* **1978**, *70*, 117.
(2) Ollis, D. F. ACS Symposium Series 518; American Chemical Society: Washington, DC, 1993.
(3) Matthews, R. W. *Water Res.* **1990**, *24*, 653.
(4) Cerrillos, C.; Adrian, M. A. P.; Navio, J. A. *J. Photochem. Photobiol., A* **1994**, *84*, 299.
(5) Navio, J. A.; Marchena, F. J.; Cerrillos, C.; Pablos, F. *J. Photochem. Photobiol., A* **1993**, *71*, 97.
(6) Wang, C. C.; Ying, J. Y. *Nanostruct. Mater.* **1997**, *9*, 583.
(7) Zhang, Z. B.; Wang, C. C.; Zakaria, R.; Ying, J. Y. *J. Phys. Chem. B* **1998,** *102*, 10871.
(8) Alfano, O. M.; Bahnemann, D.; Cassano, A. E.; Dillert, R.; Goslich, R. *Catal. Today* **2000**, *58*, 199.
(9) Serpone, N.; Lawless, D.; Didier, J.; Herrmann, J. M. *Langmuir* **1994**, *10*, 643.
(10) Che, M.; Anpo, M. *Chem. Commun.* **2001**, 435.
(11) Khairutdinov, M. *Colloid J.* **1997**, *59*, 535.
(12) Xu, Y.; Langford, C. H. *J. Phys. Chem.* **1995**, *99*, 11501.
(13) Xu, Y.; Langford, C. H. *J. Phys. Chem.* **1997**, *101*, 3115.
(14) Davydov, L.; Reddy, E. P.; France, P.; Smirniotis, P. G. *J. Catal.* **2001**, *203*, 157.
(15) Gratzel, M. *Curr. Opin. Colloid Interface Sci.* **1999**, *4*, 314.
(16) Reddy, E. P.; Davydov, L.; Smirniotis, P. G. *J. Phys. Chem. B* **2002**, *106*, 3394.
(17) Oyama, S. T.; Went, G. T.; Lewis, K. B.; Bell, A. T.; Somarjai, G. A. *J. Phys. Chem.* **1989**, *93*, 6786.
(18) Reddy, B. M.; Manohar, B.; Reddy, E. P. *Langmuir* **1993**, *9*, 1781
(19) Zang, L.; Lange, C.; Abraham, I.; Storck, S.; Maier, W. F.; Kisch, H. *J. Phys. Chem. B* **1998**, *102*, 10765.
(20) Carvalho, W. A.; Wallau, M.; Schuchardt, U. *J. Mol. Catal. A: Chem.* **1999**, *144*, 91.
(21) Hoang, D. L.; Dittmar, A.; Radnik, J.; Brzenzinka, K. W.; Witke, K. *Appl. Catal., A* **2003**, *239*, 95.
(22) Klimova, T.; Calderon, M.; Ramirej, J. *Appl. Catal., A* **2003**, *240*, 29.
(23) Wang, C. B.; Deo, G.; Wachs, I. E. *J. Catal.* **1998**, *178*, 640.
(24) Deo, G.; Wachs, I. E. *J. Catal.* **1994**, *146*, 323.
(25) Zhu, Z.; Hartman, M.; Maes, E.; Czernuszewichz, R. S.; Kevan, L. *J. Phys. Chem. B* **2000**, *104*, 4690.
(26) Dow, W. P.; Wang, Y. P.; Huang, T. J. *J. Catal.* **1996**, *160*, 155.
(27) Hoffmann, M. R.; Martin, S. T.; Choi, W.; Behnemann, D. W. *Chem. Rev.* **1995**, *95*, 69.
(28) Choi, W.; Termin, A.; Hoffmann, M. R. *J. Phys. Chem.* **1994**, *98*, 13669
(29) Yamashita, H.; Nishiguchi, H.; Kamada, N.; Anpo, M.; Teraoka, Y.; Hatano, H.; Ehara, S.; Kikui, K.; Palmisano, L.; Sclafani, A.; Schiavello, M.; Fox, M. A. *Res. Chem. Intermed.* **1994**, *20*, 815
(30) Sawada, Y.; Tamaru, H.; Kogoma, M.; Kawase, M.; Hashimoto, K. *J. Phys. D: Appl. Phys.* **1996**, *29*, 2539.